Progress In Electromagnetics Research C, Vol. 90, 1–13, 2019

Double-Port Slotted-Antenna with Multiple Miniaturized Radiators for Wideband Wireless Communication Systems and Portable Devices

Mohammad Alibakhshikenari[1, *], Mohsen Khalily[2], Bal Singh Virdee[3], Abdul Ali[1], Panchamkumar Shukla[3], Chan Hwang See[4, 5], Raed A. Abd-Alhameed[6], Francisco J. Falcone[7], and Ernesto Limiti[1]

Abstract—Proof-of-concept is presented of a novel slot antenna structure with two excitation ports. Although this antenna provides a wide impedance bandwidth, its peak gain and optimum radiation efficiency are observed at its mid-band operational frequency. The antenna structure is etched on the top side of a dielectric substrate with a ground plane. The antenna essentially consists of a rectangular patch with two dielectric slots in which multiple coupled patch arms embedded with H-shaped slits are loaded. The two dielectric slots are isolated from each other with a large H-shaped slit. The radiation characteristics of the proposed antenna in terms of impedance bandwidth, gain and efficiency can be significantly improved by simply increasing the number of radiation arms and modifying their dimensions. The antenna's performance was verified by building and testing three prototype antennas. The final optimized antenna exhibits a fractional bandwidth of 171% (0.5–6.4 GHz) with a peak gain and maximum radiation efficiency of 5.3 dBi and 75% at 4.4 GHz, respectively. The antenna has physical dimensions of $27 \times 37 \times 1.6\,\text{mm}^3$ corresponding to electrical size of $0.0452\lambda_0 \times 0.0627\lambda_0 \times 0.0026\lambda_0$, where λ_0 is freespace wavelength at 0.5 GHz. The antenna is compatible for integration in handsets and other broadband wireless systems that operate over L-, S-, and C-bands.

1. INTRODUCTION

Multiport antennas have been used in numerous applications for many years including phased array antennas and Multiple-Input-Multiple-Output (MIMO) antennas [1–3]. With the development of integrated circuit technologies, multiport antennas are more and more integrated with amplifiers, phase shifters, and other devices to realize a compact, low-loss, and multifunctional antenna system.

Various techniques have been reported over the years to implement multiport antennas [4–13]. In [10] the antenna consists of four wedge-shaped patches constructed on a grounded dielectric substrate, with each patch fed via a probe attached to a connector on the ground plane. The antenna operates over a very narrow bandwidth of 62.7 MHz centered at 2.6 GHz and radiates bi-directionally. The isolation between the ports of this antenna is better than 15 dB. The radiation patterns from individual ports are orthogonal, and beam steering can be achieved by feeding the ports simultaneously. This antenna has dimensions of $54.2 \times 44.2\,\text{mm}^2$. In [11] the antenna configuration comprises a dual feed aperture

Received 12 January 2018, Accepted 18 December 2018, Scheduled 5 January 2019
* Corresponding author: Mohammad Alibakhshikenari (alibakhshikenari@ing.uniroma2.it).
[1] Electronic Engineering Department, University of Rome "Tor Vergata", Via del Politecnico 1, Roma 00133, Italy. [2] 5G innovation Center (5GIC), Institute for Communication Systems (ICS), University of Surrey, Guildford, GU2 7XH, UK. [3] School of Computing and Digital Media, Center for Communications Technology, London Metropolitan University, London, N7 8DB, UK. [4] School of Engineering, University of Bolton, Bolton, BL3 5AB, UK. [5] School of Engineering & the Built Environment, Edinburgh Napier University, Merchiston Campus, 10 Colinton Road, Edinburgh, EH10 5DT, UK. [6] School of Electrical Engineering and Computer Science, University of Bradford, Bradford, BD7 1DP, UK. [7] Electrical and Electronic Engineering Department, Public University of Navarre, Pamplona 31006, Spain.

coupled with a square patch where a single-layer substrate is suspended 2.5 mm above another double-layer substrate. A square patch is etched on the top side of the single layer. Two bent microstriplines are fed separately from two ports on the bottom side of the double-layer substrate, where the ground-plane includes four apertures etched on the top side. The directional antenna operates over a narrow bandwidth of 163 MHz centered at 2.4 GHz and has isolation better than 30 dB between its ports. The dimensions of this antenna are $80 \times 80 \times 6.8\,\text{mm}^3$. The antenna structure in [12] resembles an elongated chevron which is etched on the top side of the substrate. It is excited by two orthogonal 50 ohm microstrip feedlines from the bottom side of the substrate. The antenna operates at 1.2 GHz and 1.7 GHz with bandwidth of −31 MHz, and radiates directionally. The isolation between the ports is better than 25 dB. It has dimensions of $60 \times 40 \times 3.2\,\text{mm}^3$. In [13] the antenna is composed of two layers of dielectric substrate and three layers of copper patches. Radiators consisting of two regular Sierpinski fractal triangles are onstructed on the top layer. The antenna contains two main ports and one auxiliary port. The two main ports are directly connected to the radiator. The auxiliary port is under the ground and feeds the radiator with an inverted-L feeding line. Ports 1 and 3 operate over the same frequency band of 1–4 GHz. The auxiliary port is multiband and operates at 2.4, 3.4, and 5.2 GHz to provide an additional WLAN/WiMAX port. Isolation between the two main ports is better than 10 dB. The isolation between the auxiliary port and the two main ports is better than 7.5 dB. The antenna has dimensions of $57 \times 40 \times 2.7\,\text{mm}^3$. The radiation efficiency of the above antennas is unspecified.

This paper presents proof-of-concept design of a novel dual-port slot antenna that is constructed on a single layer of dielectric substrate and operates over a large frequency bandwidth with a peak gain and maximum radiation efficiency at its mid-band operational frequency. Unlike conventional antenna designs, the proposed technique is not multilayered and does not employ spiral inductors, metallic via-holes and/or any other components that can exacerbate the design complexity and increase manufacturing cost. Furthermore, unlike conventional designs the very large impedance bandwidth is obtained with no impact on its physical size. The antenna's omnidirectional radiation characteristics can be enhanced by simply adding coupled radiating structures within the dielectric slots and where the radiation elements incorporate H-shaped slits. Empirical results presented of the optimization stages show how the performance of the antenna is improved. Compared to existing techniques, the proposed antenna exhibits a large fractional bandwidth of 171% (0.5–6.4 GHz) with a peak gain and maximum radiation efficiency of 5.3 dBi and 75%, respectively, at 4.4 GHz. The isolation between the ports is better than 27 dB, and the antenna has physical dimensions of $27 \times 37 \times 1.6\,\text{mm}^3$. This type of antenna with a large operational frequency range is applicable in ultra-broadband wireless systems that are rapidly evolving. The consequence of such technological developments is having to upgrade the system hardware. The proposed antenna should be able to accommodate such changes with eminent emergence of 5G mobile technology.

2. PROPOSED DUAL-PORT ANTENNA

2.1. Antenna1 with Six Miniature Radiation Arms

The geometry of the proposed antenna shown in Fig. 1 essentially consists of a large rectangular patch radiator on which are two rectangular dielectric slot cut-outs and where each slot is loaded with three identical miniature patches that are connected through a high impedance to the outer conductor. An H-shaped slit is embedded in each of the three patches. The bottom side of the substrate is a ground plane. The antenna is excited through coplanar waveguide (CPW) feed ports. The CPW is implemented by grounding the two side arms of the SMA connector. The excitation ports are separated from each other with a large H-shaped slit located in the middle of the structure which is terminated on the side with a matched 50 ohm load. The central H-shape slit that separates the two rectangular slots with the three miniature patches essentially suppresses propagation of surface currents over the antenna to thereby minimize mutual coupling between the radiation elements in the two sides of the feed ports. The slit embedded in the miniature patches enables enhanced coupling between antenna components and contributes toward the realization of a smaller structure.

The antenna was constructed on a Rogers RT/Duroid 5880 substrate with thickness of 1.6 mm, ε_r of 2.2, and $\tan\delta$ of 0.0009. Dimensions of the antenna are annotated in Fig. 1(a), i.e., $27 \times 37 \times 1.6\,\text{mm}^3$

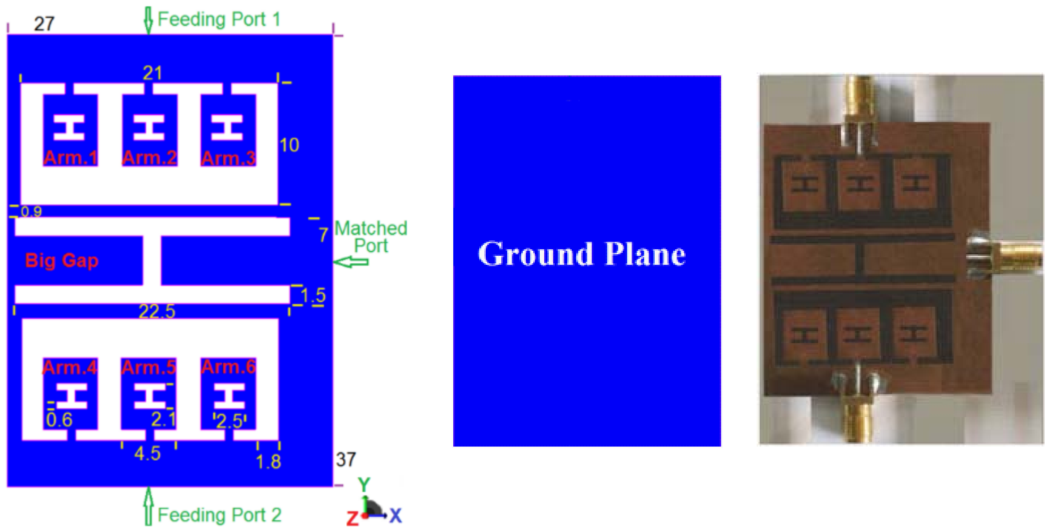

Figure 1. Configuration of the proposed Antenna-1 (dimensions annotated are in mm).

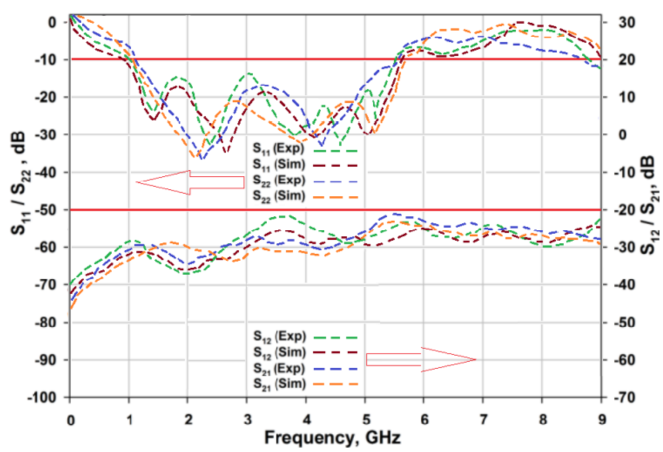

Figure 2. Simulated and measured reflection and transmission-coefficient response of Antenna-1.

or $0.0452\lambda_0 \times 0.0627\lambda_0 \times 0.0026\lambda_0$, where λ_0 is the free-space wavelength at 0.5 GHz.

The antenna's radiation characteristics were measured using the standard procedure in an anechoic chamber. The signal power was split equally to the top and bottom ports with the middle port terminated in a matched impedance of 50 ohms. The antenna gain was measured using a comparative method that involves measuring the signal received by a reference antenna and by the antenna under test (AUT), and determining the relative difference in the gain of both antennas when both the reference antenna and AUT are working in the received mode.

Simulated and measured reflection and transmission-coefficient responses of the antenna are shown in Fig. 2. The antenna was simulated using fullwave EM High Frequency Structure Simulator (HFSS). The response of the antenna is virtually the same when it is excited from either feed ports. When the antenna is excited through port-1, it has an impedance bandwidth of 4.5 GHz (1–5.5 GHz) for $S_{11} \leq -10$ dB corresponding to a fractional bandwidth of 138.46%. When it is excited through port-2, its impedance bandwidth is 4.5 GHz (1.05–5.55 GHz), and fractional bandwidth is 136.36%. There is good agreement between the simulated and measured results. The discrepancy between these results is attributed to the approximate boundary conditions in the simulation and scattering of radiation impinging on the RF cable connecting the antenna to the Agilent 8722ES vector network analyzer.

Transmission-coefficient response in Fig. 2 shows that the inter-port isolation is better than 20 dB, which is necessary to minimize mutual coupling between the ports. The simulated and measured impedance and fractional bandwidths, and inter-port isolation are given in Table 1. The simulated and measured gain and efficiency responses of the antenna in Fig. 3(a) show that the antenna has a measured peak gain and efficiency of 3.2 dBi and 57%, respectively, at 4.6 GHz. The bell-shaped gain bandwidth response resembling a reduced Q-factor profile results from the multiple radiating elements constituting the antenna. The measured gain and efficiency characteristics as a function of frequency are summarized in Table 2. The simulated and measured radiation patterns, shown in Fig. 3(b), reveal that the antenna radiates approximately omnidirectionally in both E-plane and H-planes. There is good correlation between the simulated and measured results.

Table 1. (a) Bandwidth of Antenna-1.

	Impedance Bandwidth/ Frequency range	Fractional Bandwidth
Exp. (S_{11})	4.5 GHz/(1–5.50 GHz)	$\approx$ 138%
Sim. (S_{11})	4.7 GHz/(0.95–5.65 GHz)	$\approx$ 142%
Exp. (S_{22})	4.5 GHz/(1.05–5.55 GHz)	$\approx$ 136%
Sim. (S_{22})	4.7 GHz/(1.00–5.70 GHz)	$\approx$ 140%

(b) Port isolation of Antenna-1.

Exp. (S_{12})	$\geq$ 20 dB
Sim. (S_{12})	$\geq$ 25 dB
Exp. (S_{21})	$\geq$ 20 dB
Sim. (S_{21})	$\geq$ 22 dB

Table 2. Gain and efficiency of Antenna-1.

Frequency (GHz)	Gain (dBi)	Efficiency (%)
1.00	0.8	20
1.50	1.2	27
2.38	1.8	34
3.80	2.5	44
4.60	3.2	57
5.20	3.0	53
5.50	2.9	50

2.2. Antenna-2 with Ten Miniature Radiation Arms

The size and structure of Antenna-2 is identical to Antenna-1, shown in Fig. 1, with (i) the inclusion of four additional miniature radiation patches with H-slits; (ii) the reduction in the inter-port gap; and (iii) the reduction in the inter-port H-slit, as shown in Fig. 4. The simulated and measured reflection and transmission-coefficient responses of Antenna-2, shown in Fig. 5, reveal improvement in the antenna's performance by introducing these changes, which is attributed to reduction in the antenna's Q-factor. When the antenna is excited through port-1, its impedance bandwidth improves to 5.2 GHz (0.8–6 GHz) for $S_{11} \leq -10$ dB, with a corresponding fractional bandwidth 152.94%. When the antenna is excited through port-2, its bandwidth is 5.2 GHz (0.85–6.05 GHz), and the corresponding fractional bandwidth is 150.72%. The transmission-coefficient in Fig. 5 shows that the inter-port isolation is better than 25 dB.

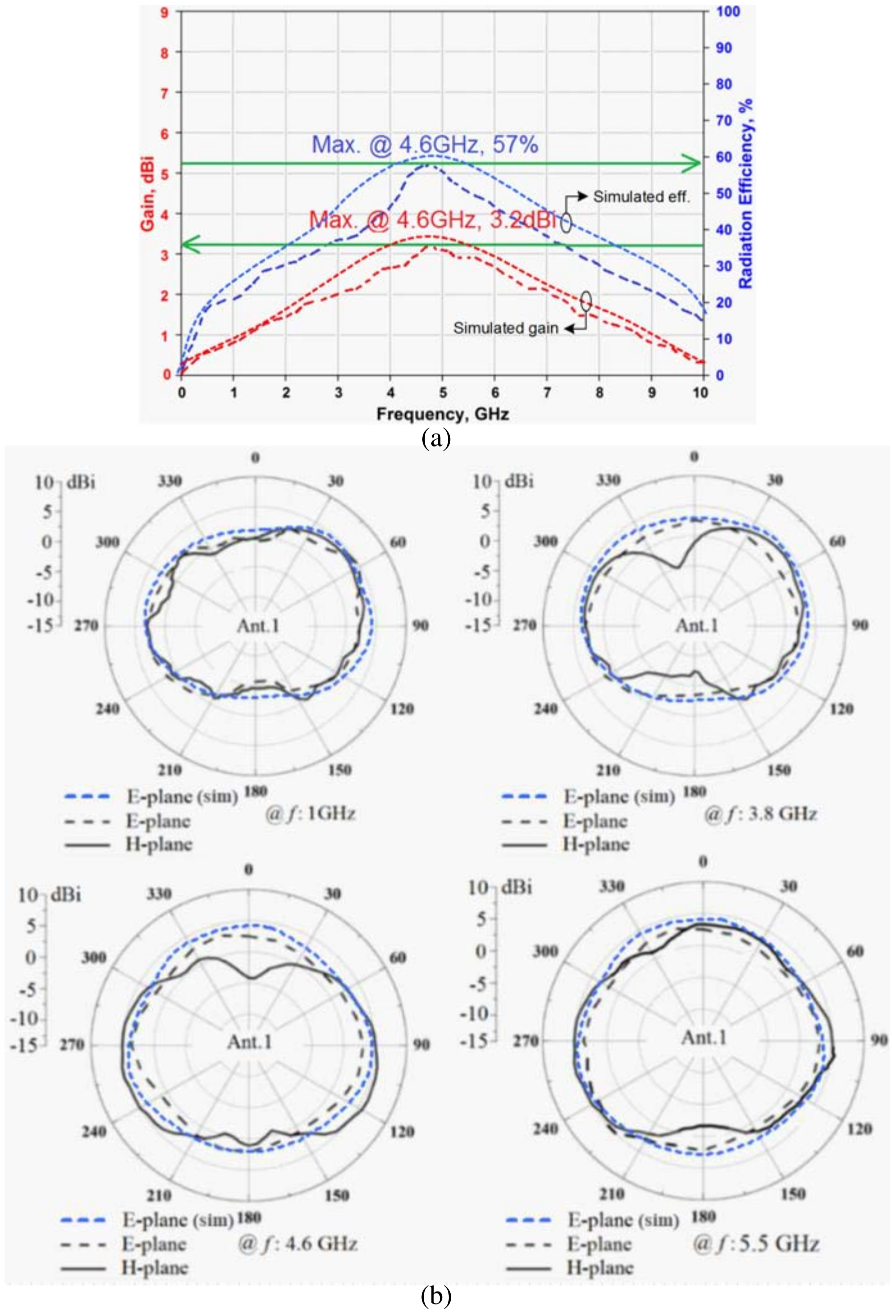

Figure 3. Radiation properties of the Antenna 1. (a) Simulated and measured gain and efficiency response of Antenna-1 throughout frequency. (b) Simulated and measured E-plane and H-plane radiation patterns of Antenna-1.

The impedance and fractional bandwidths, and inter-port isolation are given in Table 3. The simulated and measured gain and efficiency responses of the antenna are shown in Fig. 6(a). This graph shows the antenna's measured peak gain and efficiency improve to 4.7 dBi and 66%, respectively, at 4.7 GHz. The measured gain and efficiency characteristics as a function of frequency are summarized in Table 4.

The antenna's simulated and measured radiation patterns, shown in Fig. 6(b), are significantly better than Antenna-1. The antenna radiates omnidirectionally in both E- and H-planes.

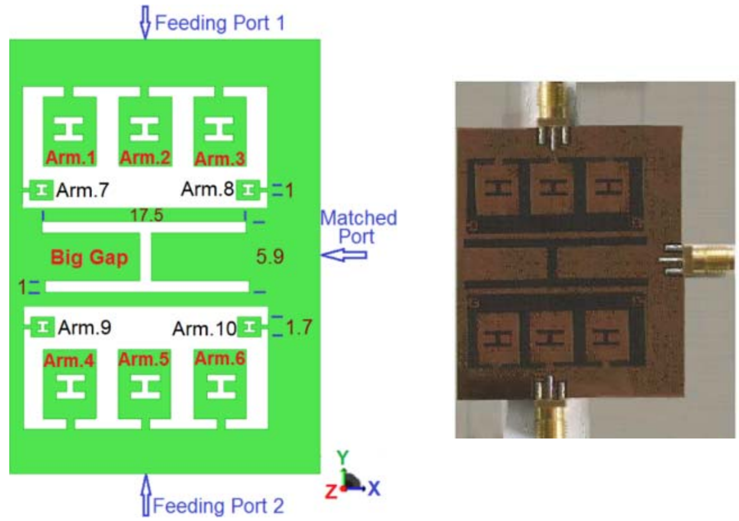

Figure 4. Antenna-2 loaded with ten radiation arms (dimensions annotated are in mm). All other dimensions are same as Antenna-1. As well as, Antenna-2 has same ground plane with Antenna-1 shown in Fig. 1.

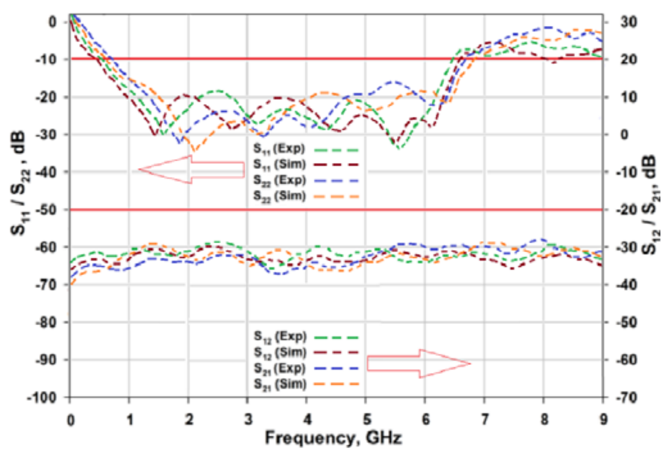

Figure 5. Simulated and measured reflection-coefficient response of Antenna-2.

2.3. Antenna-3 with Optimized Parameters

Further improvement in the antenna's characteristics was achieved by enlarging the four side patch arms and shortening the size of the central H-slit, as shown in Fig. 7. Dimensions of all other antenna parameters are identical to Antenna-1. Fig. 8 shows that the reflection and transmission-coefficient responses of Antenna-3 are improved compared to Antennas-1 and -2. When Antenna-3 is excited through port-1, its impedance bandwidth is now improved to 5.9 GHz (0.5–6.4 GHz) for $S_{11} \leq -10\,\text{dB}$,

Table 3. (a) Bandwidth of Antenna-2.

	Impedance Bandwidth/Frequency range	Fractional Bandwidth
Exp (S_{11})	5.2 GHz/(0.80–6.00 GHz)	$\approx$ 152%
Sim. (S_{11})	5.4 GHz/(0.75–6.15 GHz)	$\approx$ 156%
Exp. (S_{22})	5.2 GHz/(0.85–6.05 GHz)	$\approx$ 150%
Sim. (S_{22})	5.45 GHz/(0.8–6.20 GHz)	$\approx$ 154%

(b) Port isolation of Antenna-2.

Exp (S_{12})	≤ -25 dB
Sim. (S_{12})	≤ -25 dB
Exp (S_{21})	≤ -27 dB
Sim. (S_{21})	≤ -26 dB

Table 4. Gain and efficiency of Antenna-2.

Frequency (GHz)	Gain (dBi)	Efficiency (%)
0.8	0.7	21
1.2	1.5	33
2.2	2.4	41
2.8	2.9	50
3.8	3.5	58
4.7	4.1	66
5.6	3.8	61
6	3.2	55

Table 5. (a) Bandwidth of Antenna-3.

	Impedance Bandwidth/Frequency range	Fractional Bandwidth (%)
Exp. (S_{11})	5.9 GHz/(0.50–6.40 GHz)	≈ 171
Sim. (S_{11})	6.2 GHz/(0.40–6.60 GHz)	≈ 177
Exp. (S_{22})	5.9 GHz/(0.55–6.45 GHz)	≈ 169
Sim. (S_{22})	6.3 GHz/(0.45–6.55 GHz)	≈ 175

(b) Port isolation of Antenna-3.

Exp. (S_{12})	≥ 28 dB
Sim. (S_{12})	≥ 30 dB
Exp. (S_{21})	≥ 27 dB
Sim. (S_{21})	≥ 28 dB

and consequently its fractional bandwidth improves to 171.01%. When the antenna is excited through port-2, the antenna bandwidth is 5.9 GHz (0.55–6.45 GHz), and its fractional bandwidth is 168.57%. Fig. 8 also shows that the antenna's inter-port isolation is better than 27 dB. The impedance, fractional bandwidth and inter-port isolation are given in Table 5.

The simulated and measured gain and efficiency responses of the antenna are shown in Fig. 9(a). This graph shows the antenna's measured peak gain and efficiency improve to 5.3 dBi and 75%, respectively, at 4.4 GHz. The measured gain and efficiency characteristics as a function of frequency are summarized in Table 6. The antenna radiates essentially omnidirectionally in both E- and H-planes as shown in Fig. 9(b).

The optimized design is compared with existing state-of-the-art designs in terms of size, bandwidth, and radiation specifications in Table 7. The results show that the proposed antenna covers a wider frequency band than other antennas, and its radiation characteristics, such as gain and efficiency, are comparable to the references cited in Table 7. However, unlike other designs the dimensions of the proposed antenna structure remain unaffected when its impedance bandwidth is increased.

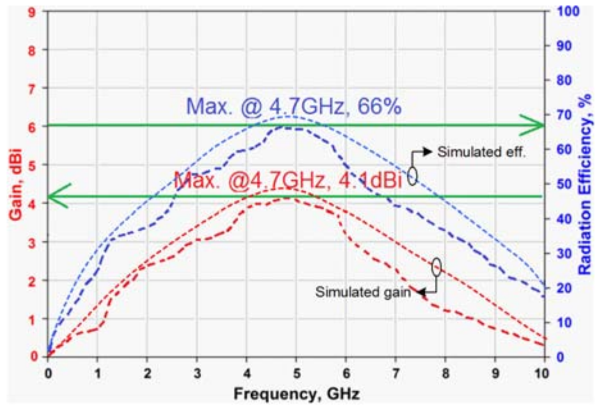

(a)

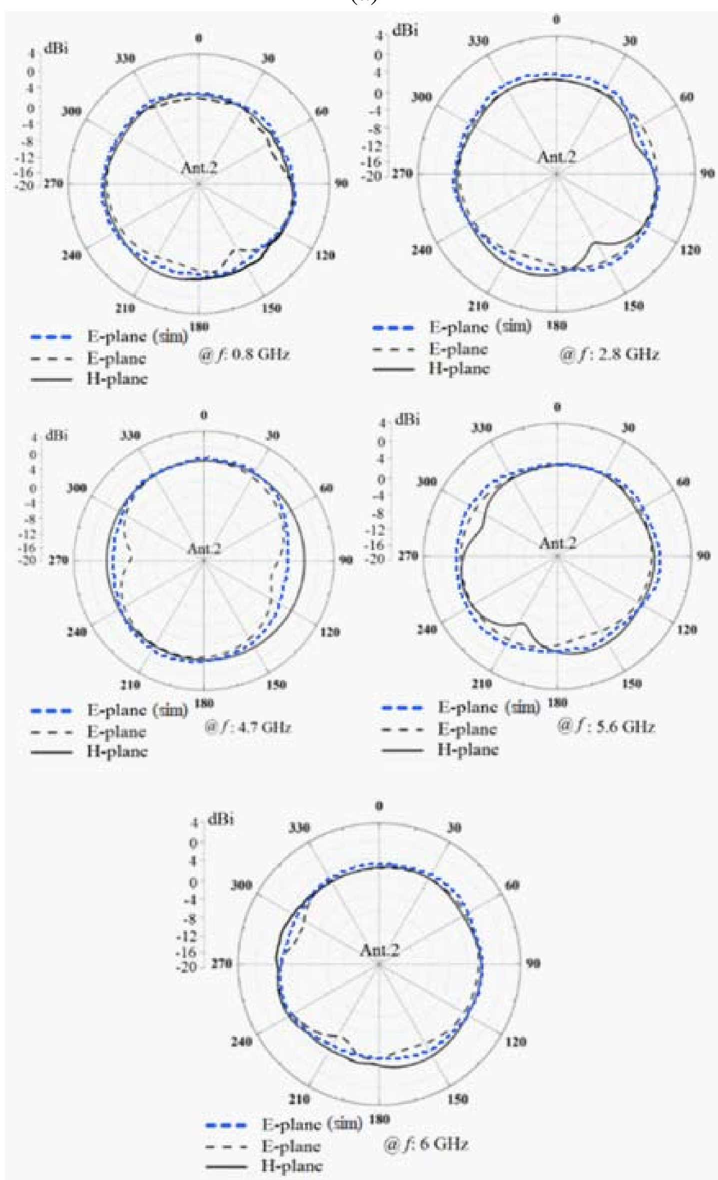

(b)

Figure 6. Radiation characteristics of the Antenna-2. (a) Simulated and measured gain & efficiency response of Antenna-2 over frequency. (b) Simulated and measured E-plane and H-plane radiation patterns of Antenna-2.

Table 6. Gain and efficiency of Antenna-3.

Frequency (GHz)	Gain (dBi)	Efficiency (%)
0.5	0.4	15
0.7	0.8	20
1.1	1.6	35
2	2.5	44
2.5	3.2	50
3.7	4.1	62
4.4	5.3	75
5.2	4.8	71
6.05	4.3	64
6.4	4.0	59

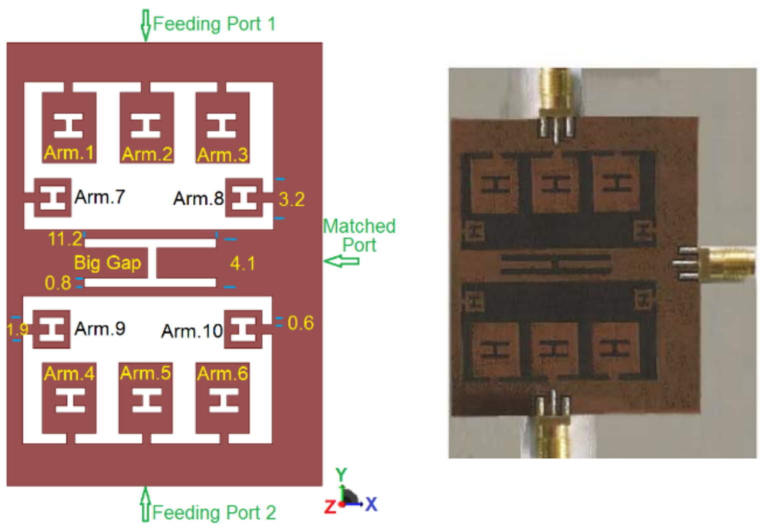

Figure 7. Antenna-3 loaded with four side radiating patches, central H-slit and inter-port gap (dimension annotated are in mm). All other dimensions are same as Antenna-1. In addition, Antenna-3 has same ground plane with Antenna-1 shown in Fig. 1.

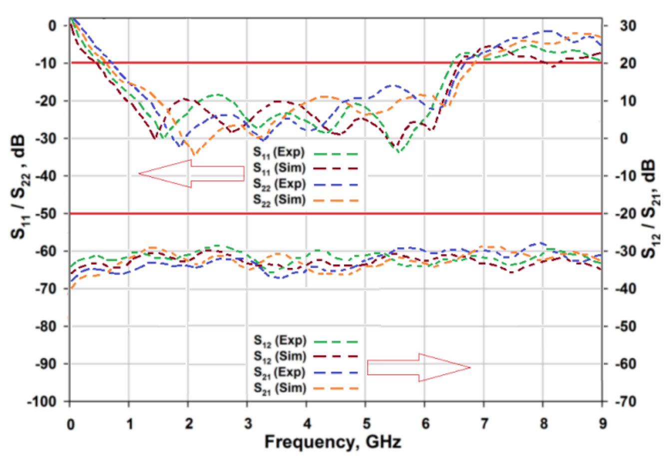

Figure 8. Simulated and measured reflection and transmission-coefficient response of Antenna-3.

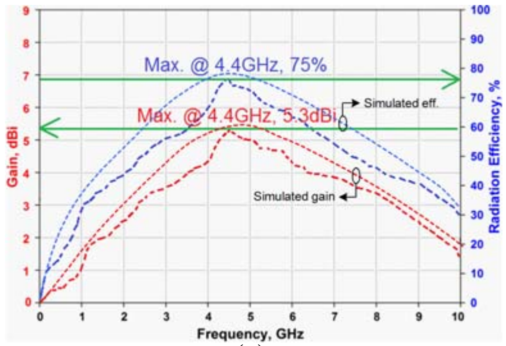

(a)

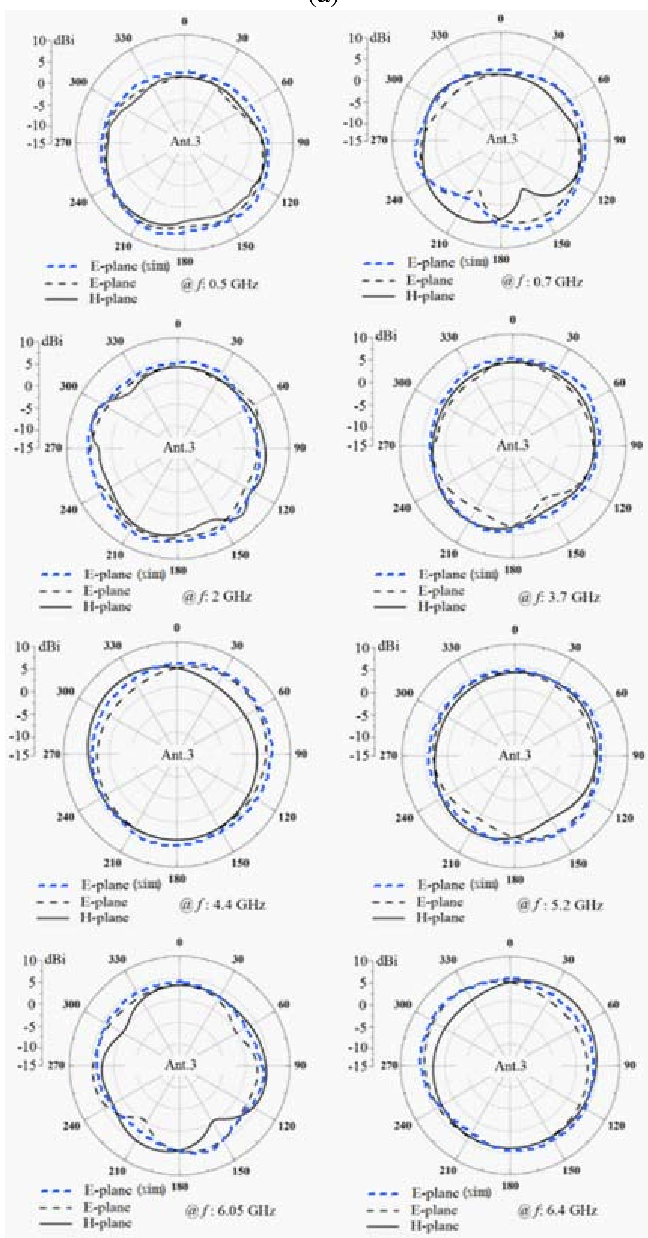

(b)

Figure 9. Radiation specifications of the Antenna3. (a) Simulated and measured gain and efficiency response of Antenna-3 versus frequency. (b) Simulated and measured E-plane and H-plane radiation patterns of Antenna-3.

Table 7. Characteristics of the proposed antenna compared with state-of-the-art designs. FBW represents the fractional bandwidth.

Ref.	Size (mm^3)	Bandwidth	Gain	Peak Efficiency
[8] H-shaped antenna	$15 \times 6.9 \times 0.8$	1.2–6.7 GHz (FBW: $\sim$ 140%)	6.8 dBi	86%
[8] T-shaped antenna	$15.5 \times 6.9 \times 0.8$	1.1–6.85 GHz (FBW: $\sim$ 145%)	7.1 dBi	91%
[14]	$10 \times 35 \times 0.4$	3.1–5.0 GHz (FBW: $\sim$ 47%)	-	-
[15]	$30 \times 15 \times 0.5$	3.0–5.4 GHz (FBW: 57%)	5 dBi	98%
[16]	$57 \times 37.5 \times 0.8$	1.7–3.1 GHz (FBW: 58%)	2.8 dBi	-
[17]	$10.1 \times 10.1 \times 1.5$	0.43–0.5 GHz (FBW: 15%)	-	-
[18]	$7.5 \times 13.5 \times 1.6$	3.45–3.65 GHz (FBW: 5.6%); 4.65–8.7 GHz (FBW: 60.67%)	4 dBi	-
[19]	$44 \times 25 \times 0.8$	2.3–2.4 GHz (FBW: 4.25%); 2.5–2.7 GHz (FBW: $\sim$ 8%); 2.40–2.485 (FBW: $\sim$ 3.5%); 3.4–3.6 GHz (FBW: $\sim$ 6%)	-	-
[20]	$21.6 \times 19.8 \times 0.8$	0.7–8 GHz (FBW: 167.8%)	4 dBi	80%
[21]	$60 \times 16 \times 1$	0.67–2.55 GHz (FBW: 116.7%)	4.74 dBi	62.9%
[22]	$18 \times 18 \times 1.6$	1.8–2.35 GHz (FBW: 26.5%)	3.69 dBi	20%
[23]	$60 \times 5 \times 5$	0.8–2.5 GHz (FBW: 103%)	0.45 dBi	53.6%
[24]	$18.2 \times 18.2 \times 6.5$	1–2 GHz (FBW: 66.7%)	0.6 dBi	26%
[25]	$12 \times 12 \times 3.33$	2.34–2.54 GHz (FBW: 8.2%)	1 dBi	22%
[26]	$20 \times 25 \times 0.8$	3.45–3.75 GHz (FBW: 8.3%)	2 dBi	27%
Proposed Design	$\mathbf{27 \times 37 \times 1.6}$	**0.5–6.4 GHz (FBW: 171%)**	**5.3 dBi**	**75%**

Metamaterial techniques are used in [8] & [20] to improve the antenna's performances. Left-handed metamaterial structure in [8] is realized with spiral inductors that are connected to the ground plane by metallic via-holes, and the antenna structure in [20] needs to be terminated in 50-ohm load. The proposed antenna avoids the use of spiral inductors and metallic via-holes or load termination which introduce additional design complexity and therefore increase fabrication cost.

The proposed antenna operates over a wide frequency range from 500 MHz to 6.4 GHz, which covers L-, S- and C-bands. Hence, the antenna can be used for multiband wireless systems that encompass GPS, mobile phones, WiFi/WLAN, satellite communications, and WiMAX.

3. CONCLUSION

A novel dual-port slot antenna structure which is implemented with multiple miniature patch radiators is shown to exhibit broadband performance. The antenna structure is etched on the top side of a dielectric substrate, and the ground-plane is on the bottom side of the substrate. An H-shaped slit is embedded in the radiators to concentrate the EM fields and currents over the patches to enhance coupling between the neighboring radiators. The proposed antenna allows the bandwidth, gain and efficiency to be improved by simply modifying the dimensions of the miniature radiators and slits without compromising the antenna's overall size. Effective isolation between the feed ports is realized with the inclusion of an H-shaped slit between the ports. The optimized antenna provides a fractional bandwidth of 171% (0.5–6.4 GHz) with a peak gain and maximum radiation efficiency of 5.3 dBi and 75%, respectively, at 4.4 GHz. The isolation between the ports is better than 27 dB. The proposed dual-port slot antenna is compatible for integration in handsets and broadband wireless systems.

ACKNOWLEDGMENT

This work is partially supported by innovation programme under grant agreement H2020-MSCA-ITN-2016 SECRET-722424.

REFERENCES

1. Mailloux, R., *Phased Array Antenna Handbook*, Artech House, Norwood, MA, 2005.
2. Browne, D. W., M. Manteghi, M. P. Fitz, and Y. Rahmat-Samii, "Experiments with compact antenna arrays for MIMO radio communications," *IEEE Trans. Antennas Propag.*, Vol. 54, No. 11, 3239–3250, Nov. 2006.
3. Rembold, B., "Relation between diagram correlation factors and parameters of multiport antenna with arbitrary feeding network," *Electron. Lett.*, Vol. 44, No. 1, 5–7, Jan. 2008.
4. Liu, J., Y. Cheng, Y. Nie, and R. Gong, "Metamaterial extends microstrip antenna," *Microwaves & RF.*, Vol. 52, No. 12, 69–73, 2013.
5. Arora, C., S. S. Pattnaik, and R. N. Baral, "Dual band microstrip patch antenna array loaded with split ring resonators and via holes," *AEU — Int. Journal of Electronics and Communications*, Vol. 93, 253–260, Sept. 2018.
6. Rezvani, M. and Y. Zehforoosh, "A dual-band multiple-input multiple-output microstrip antenna with metamaterial structure for LTE and WLAN applications," *AEU — Int. Journal of Electronics and Communications*, Vol. 93, 277–282, Sept. 2018.
7. Cheng, Y. Z., Y. L. Yang, Y. J. Zhou, Z. Zhang, X. S. Mao, and G. R. Zhou, "Indefinite-permeability metamaterial lens with finite size for miniaturized wireless power transfer system," *AEU — Int. Journal of Electronics and Communications*, Vol. 70, No. 9, 1282–1287, 2016.
8. Alibakhshi-Kenari, M., M. Naser-Moghadasi, R. A. Sadeghzadeh, and B. S. Virdee, "Metamaterial-based antennas for integration in UWB transceivers and portable microwave handsets," *Int. Journal of RF and Microwave Computer-Aided Engineering*, Vol. 26, No. 1, 88–96, Jan. 2016.
9. Alibakhshi-Kenari, M., M. Naser-Moghadasi, R. A. Sadeghzadeh, B. S. Virdee, and E. Limiti, "Dual-band RFID tag antenna based on the Hilbert-curve fractal for HF and UHF applications," *IET Circuits, Devices & Systems*, Vol. 10, No. 2, 140–146, Mar. 2016.
10. Coetzee, J. C. and Y. Liu, "Compact multiport antenna with isolated ports," *Microwave and Optical Tech. Letters*, Vol. 50, No. 1, 229–232, 2006.

11. Wang, B., Y. Zhuang, and X. Li, "Compact dual ports handheld RFID reader antenna with high isolation," *Int. Journal of RF and Microwave Computer-Aided Engineering*, Vol. 25, No. 6, 548–555, 2015.
12. Paulson, M., S. O. Kundukulam, C. K. Aanandan, and P. Mohanan, "Analysis and design of a dual-port compact microstrip antenna," *Microwave and Optical Tech. Letters*, Vol. 32, No. 2, 125–127, 2002.
13. Wang, R., B.-Z. Wang, Z.-S. Gong, and X. Ding, "Compact multiport antenna with radiator-sharing approach and its performance evaluation of time reversal in an intra-car environment," *IEEE Trans. on Antennas and Propagation*, Vol. 63, No. 9, 4213–4219, 2015.
14. Chang, Y.-C. and C.-C. Chiu, "Design of a planar ultra-wideband miniature monopole antenna for wireless USB dongle devices," *Microwave and Optical Technology Letters*, Vol. 52, No. 5, 1013–1016, May 2010.
15. See, C. H., R. A. Abd-Alhameed, D. Zhou, H. I. Hraga, and P. S. Excell, "Miniature dual-band and wideband planar inverted F-L-antennas for wireless local area network and ultra-wideband applications," *Electromagnetics*, Vol. 31, No. 3, 233–245, DOI: 10.1080/02726343.2011.558462.
16. Hraga, H. I., C. H. See, R. A. Abd-Alhameed, D. Zhou, S. Adnan, I. T. E. Elfergani, and P. S. Excell, "Small wideband antenna for GSM and WLAN applications," *Fourth European Conference on Antennas and Propagation (EuCAP)*, Barcelona, Spain, Apr. 12–16, 2010.
17. Kwak, S. I., K. Chang, and Y. J. Yoon, "Small spiral antenna for wideband capsule endoscope system," *Electronics Letters*, Vol. 42, No. 23, 1328–1329, 2006.
18. Naidu, P. V., A. Kumar, and V. Kumar, "A very small wideband asymmetric coplanar strip fed printed dual band antenna for advanced communication applications," *2017 Progress In Electromagnetics Research Symposium — Fall (PIERS — FALL)*, Singapore, Nov. 19–22, 2017.
19. Saini, H. S., A. Thakur, R. Kumar, A. Sharma, and N. Kumar, "A small size wideband planar inverted-F antenna für usb düngle devices," *1st IEEE Int Conference on Power Electronics. Intelligent Control and Energy Systems (ICPEICES-2016)*, 2016.
20. Alibakhshi-Kenari, M., M. Naser-Moghadasi, R. A. Sadeghzadeh, B. S. Virdee, and E. Limiti, "New compact antenna based on simplified CRLH-TL for UWB wireless communication systems," *Int. Journal of RF and Microwave Computer-Aided Engineering*, Vol. 26, No. 3, 217–225, Mar. 2016.
21. Luo, J., S. Gong, P. Duan, C. Mou, and M. Long, "Small-size wideband monopole antenna with CRLH-TL for LTE mobile phone," *Progress In Electromagnetics Research C*, Vol. 50, 171–179, 2014.
22. Abdalla, M. A., A. A. Awad, and K. M. Hassan, "Wide band high selective compact metamaterial antenna for 2 GHz wireless applications," *Antennas and Propagation Conf.*, 350–354, Loughborough, Leicestershire, United Kingdom, Nov. 2014.
23. Li, Y., Z. Zhang, J. Zheng, and Z. Feng, "Compact heptaband reconfigurable loop antenna for mobile handset," *IEEE Antennas Wireless Propag. Lett.*, Vol. 10, 1162–1165, 2011.
24. Lee, C. J., K. M. K. H. Leong, and T. Itoh, "Composite right/lefthanded transmission line based compact resonant antennas for RF module integration," *IEEE Trans. Antennas Propag.*, Vol. 54, 2283–2291, 2006.
25. Lee, C. J., K. M. H. Leong, and T. Itoh, "Broadband small antenna for portable wireless application," *Int. Workshop on Antenna Technology: Small Antennas and Novel Metamaterials, iWAT 2008*, 10–13, Mar. 4–6, 2008.
26. Yu, C.-C., M.-H. Huang, L.-K. Lin, and Y.-T. Chang, "A compact antenna based on metamaterial for WiMAX," *Asia-Pacific Microwave Conference*, Macau, China, Dec. 2008.